Optics Letters

Undersampling for fiber distributed acoustic sensing based on coherent phase-OTDR

Fei Jiang,[1,2] Honglang Li,[2,*] Zhenhai Zhang,[1] Zhewen Hu,[3] Yanzhu Hu,[4] Yixin Zhang,[5] and Xuping Zhang[5]

[1]School of Mechatronics Engineering, Beijing Institute of Technology, Beijing 100081, China
[2]Institute of Acoustics, Chinese Academy of Sciences, Beijing 100190, China
[3]School of Optical and Electronic Information, Huazhong University of Science and Technology, Wuhan 430074, China
[4]School of Automation, Beijing University of Posts and Telecommunications, Beijing 100876, China
[5]The Key Laboratory of Intelligent Optical Sensing and Manipulation, Nanjing University, Nanjing 210008, China
*Corresponding author: lhl@mail.ioa.ac.cn

Received 14 November 2018; revised 9 January 2019; accepted 14 January 2019; posted 14 January 2019 (Doc. ID 351919); published 8 February 2019

Phase-sensitive optical time-domain reflectometry (φ-OTDR) based on coherent detection is one of the most widely used schemes to achieve fiber distributed acoustic sensing. In previous studies, a fairly high data acquisition speed is essential for the phase-measuring coherent φ-OTDR, thus leading to a severe computational burden. In this Letter, we first analyze the power spectrum of the beat signal and then propose the use of undersampling theory to reduce the need for high sampling frequency. Then we give the principle of selecting the matched sampling frequency and bandpass filter bandwidth so that the beat signal can be sampled without aliasing. The experimental results show that, when the central frequency of the beat signal is 200 MHz, its phase signal can be correctly demodulated even using a sampling rate as low as 71 MSa/s. This method can be extended to all existing coherent φ-OTDR systems with no or only a few modifications on them.

https://doi.org/10.1364/OL.44.000911

Fiber distributed acoustic sensing (DAS) based on phase-sensitive optical time-domain reflectometry (φ-OTDR) has been widely used in many fields such as perimeter security [1,2], structure health monitoring [3], and pipeline monitoring [4] due to the high sensitivity, low cost, long sensing range, and distributed capability. In φ-OTDR systems, narrow linewidth optical pulses are injected into the sensing fiber, and Rayleigh backscattering (RBS) light is produced as a result. External perturbations applied to the sensing fiber will change the refractive index and length of the fiber, thus leading to amplitude and phase change of the RBS lightwave. Traditional φ-OTDR systems only demodulate the amplitude of the RBS lightwave to detect the vibration events. However, there exists a severe nonlinear property in amplitude-measuring φ-OTDR systems; thus, the recovered acoustic signal may be distorted. Extracting the phase signal of the RBS lightwave can solve this problem.

In recent years, various phase extraction schemes for φ-OTDR have been proposed. In Refs. [5,6], the phase change induced by external perturbations is obtained by calculating the cross-correlation between two frequency scanning circles. Moreover, a chirped pulses' scheme [7,8] has been used to obtain the quantitative information of the disturbances in a single shot. Some researchers introduced an interferometer in the φ-OTDR to demodulate the phase of the RBS lightwave. An interferometer combined with a 3×3 optical coupler is used in Refs. [9–12], while an unbalanced Michelson interferometer combined with the phase-generated carrier (PGC) technology is used in Refs. [13–15]. Some researchers applied dual-pulse probes to get the quantitative information for the φ-OTDR-based DAS system [16–20]. In addition, [21] proposed a scheme based on I/Q demodulation and homodyne detection using a 90° optical hybrid. Ref. [22] proposed a phase demodulation method that used only the pure direct detection system.

Coherent detection is one of the most widely used phase extraction schemes for φ-OTDR-based DAS systems due to its simple configuration and long sensing range. Since [23] proposed the phase demodulating method based on digital coherent detection, much attention has been paid to improving the robustness of phase demodulation. Ref. [24] proposed a statistic calculation method to suppress the demodulation error. Ref. [25] introduced a series of auxiliary weak reflection points along the fiber to compensate the phase noise in the φ-OTDR so that the phase signal can be well extracted even under long sensing range. Ref. [27] proposed that by comparing the demodulated phase of the RBS lightwave before and behind the alarm location, the false alarms can be distinguished from real vibrations. Ref. [29] pointed out that the section for differential phase calculation must cover at least the whole vibration region together with a section of fiber spaced by a pulse duration. It should be noted that, in all of these literatures, a fairly high sampling rate (at least 500 MSa/s [25]) was used to well recover the beat signal for phase demodulation. However, such a high data generating speed could lead to computational burden,

which greatly limits the feasibility of realizing real-time phase demodulation for DAS systems.

In this Letter, we introduce the undersampling theory for coherent φ-OTDR systems to reduce the high sampling frequency requirement without any information loss. We first analyze the power spectrum of the beat signal in the coherent φ-OTDR. Then according to the beat signal bandwidth and the undersampling theory, we give the principle of matching the correct sampling frequency to avoid aliasing. Finally, we conduct two experiments to demonstrate the validity of using undersampling in the coherent φ-OTDR.

In φ-OTDR systems, the RBS lightwave can be expressed by using the backscatter impulse model [31]. When an optical pulse with pulse width W is launched into the fiber, the electric field of the RBS lightwave can be expressed as

$$E_R(t) = E_r \sum_{i=1}^{N} r_i \,\mathrm{rect}\left(\frac{t-\tau_i}{W}\right) \times \exp\{j[2\pi(f_0+\Delta f)(t-\tau_i)] + \varphi_0 + \phi_i\}, \quad (1)$$

where $r_i = a_i \exp(-\alpha v \tau_i)$, α is the optical power attenuation coefficient, v refers to the velocity of light in the fiber, a_i, ϕ_i, and τ_i are the amplitude, phase, and relative delay of the ith scatterer, respectively, E_r, f_0, and φ_0 are the electric field intensity, frequency, and initial phase of the incident light, respectively, Δf is the frequency shift induced by the acousto-optic modulator (AOM), and N is the total number of scatterers. The propagating rectangular pulse is defined as $\mathrm{rect}[(t-\tau_i)/W]=1$ for $0 \le (t-\tau_i)/W \le 1$ and 0 otherwise. External perturbations near the ith scatterer may change the phase ϕ_i. The electric field of the local reference lightwave can be expressed as

$$E_L(t) = E_l \exp[j(2\pi f_0 t + \varphi_t)], \quad (2)$$

where E_l is the electric field intensity of the local reference light, and φ_t denotes the phase noise of the laser. The local reference lightwave is mixed with the RBS lightwave returned from the sensing fiber, resulting in a beat light. The AC component of the beat light is detected by a balanced photodetector (BPD). The electrical output of the BPD can be expressed as

$$I(t) = 2E_l E_r \sum_{i=1}^{N} r_i \,\mathrm{rect}\left(\frac{t-\tau_i}{W}\right) \cos(2\pi\Delta f t + \Delta\varphi_i), \quad (3)$$

where $\Delta\varphi_i = -2\pi(f_0+\Delta f)\tau_i + \varphi_0 - \varphi_t + \phi_i$. The autocorrelation function of $I(t)$ can be expressed as

$$R_{\mathrm{II}}(T) = E[I(t)I(t-T)] \simeq 2E_l^2 E_r^2 W \overline{a^2} \times \exp(-2\alpha v t)\,\mathrm{tri}(T/W)\cos(2\pi\Delta f T), \quad (4)$$

where $\overline{a^2} = E[a_i^2]$, $\mathrm{tri}(T/W) = 1-|T|/W$ for $|T| < W$ and 0 otherwise. According to the Wiener–Khinchin theorem, the instantaneous power spectrum of the beat signal can be given by calculating the Fourier transform of Eq. (4):

$$S(t,f) \simeq 2E_l^2 E_r^2 W^2 \overline{a^2} \exp(-2\alpha v t)\,\mathrm{sinc}^2[(f \pm \Delta f)W], \quad (5)$$

where $\mathrm{sinc}(x) = \sin(\pi x)/(\pi x)$. Therefore, the central frequency and main lobe width of the beat signal power spectrum equals to Δf and $2/W$, respectively. The full width at half-maximum (FWHM) of the beat signal power spectrum can be approximately given as $0.8859/W$.

It is well known that when a signal [whose spectrum is $F(\omega)$] is sampled with sampling frequency ω_S, the spectrum of the sampled signal can be expressed as

$$F_S(\omega) = \omega_S \sum_{n=-\infty}^{\infty} F(\omega - n\omega_S), \quad (6)$$

where $n = 0, \pm1, \pm2, \ldots$. If a signal's frequency band is not adjacent to zero frequency, as shown in Fig. 1(a), it can be called a bandpass signal. We assume that ω_C and $2\omega_B$ are the central frequency and bandwidth of the bandpass signal, respectively, while ω_L and ω_U represent the lower and upper cutoff frequencies, respectively. If we use a sampling frequency lower than $2\omega_U$ to sample the bandpass signal, it can be regarded as an undersampling process. Figures 1(b)–1(d) show three typical types of spectrums of the sampled signals when different sampling frequencies are used. We can see from Fig. 1(b) that when the sampling frequency ω_S is not properly used, the spectrum of the sampled signal could be aliasing, whereas spectrum aliasing does not exist when ω_S is set correctly, as shown in Figs. 1(c) and 1(d). Gaskill [32] yielded the range of sampling frequencies for which no aliasing occurs:

$$\frac{2\omega_U}{n} \le \omega_S \le \frac{2\omega_L}{n-1}, \quad (7)$$

where n is an integer given by $1 \le n \le \omega_U/2\omega_B$. Liu *et al.* [33] also pointed out that the placement of the spectrum is normal [shown in Fig. 1(c)] if n is odd and inverse [shown in Fig. 1(d)] if n is even. It should be noted that when undersampling a real-world signal using a data acquisition card (DAQ), the analog input bandwidth of the DAQ should be larger than the maximum signal frequency so that the signal can be captured by the sampling circuit.

In coherent φ-OTDR systems, a bandpass filter (BPF) is usually used after the BPD to suppress out-of-band noise of the beat signal, resulting in a bandpass signal. Assuming that the bandwidth of the BPF used after the BPD is equal to B, according to Eq. (7), the optional sampling frequency f_S for the system should meet

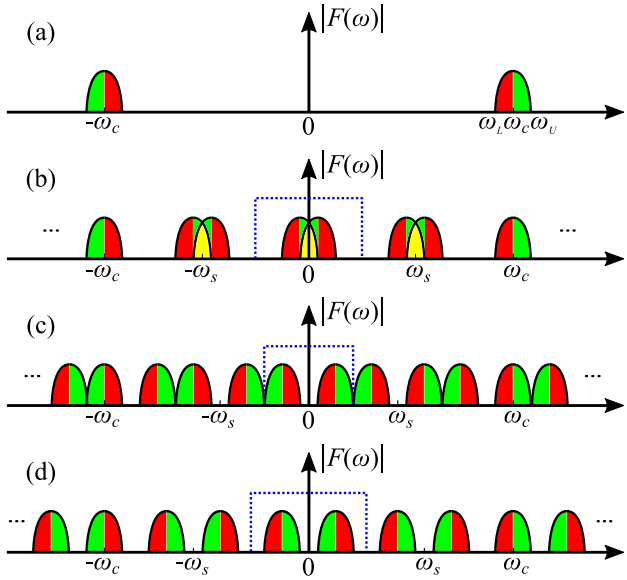

Fig. 1. Spectrum distribution before and after undersampling. (a) The spectrum of a bandpass signal. (b) The spectrum of sampled signal with aliasing. (c) The normal spectrum of sampled signal without aliasing. (d) The inverse spectrum of sampled signal without aliasing.

$$\frac{2\Delta f + B}{n} \le f_S \le \frac{2\Delta f - B}{n-1}, \tag{8}$$

where n is an integer given by $1 \le n \le (2\Delta f + B)/2B$. Therefore, to avoid aliasing, the sampling frequency and the BPF bandwidth should match the relationship given by Eq. (8). Typically, when the frequency shift induced by an AOM is 200 MHz, the allowed sampling frequency and the BPF bandwidth are shown in Fig. 2. The green and red areas represent normal and inverse spectrum placement, respectively. We can see that the narrower the BPF bandwidth, the lower the sampling frequency that can be used. However, it should be noted that the BPF bandwidth should be wider than the FWHM of the beat signal spectrum so that most of the signal energy can be kept. In conclusion, the sampling frequency selection depends on the BPF bandwidth, while the lower bound of the BPF bandwidth is determined by the optical pulse width ($B \ge 0.8859/W$).

The sampled beat signal can be simply described as follows:

$$I_s(t) = A(t)\cos[2\pi f_c t + \phi(t)], \tag{9}$$

where $A(t)$ and $\phi(t)$ are the amplitude and phase of the RBS lightwave, respectively. The carrier frequency f_c depends on the sampling frequency and the integer n used in Eq. (8), which is given by

$$f_c = \begin{cases} \Delta f - \frac{n-1}{2} f_s & n = 1, 3, 5, \ldots \\ -\Delta f + \frac{n}{2} f_s & n = 2, 4, 6, \ldots \end{cases}. \tag{10}$$

We can then demodulate the amplitude and phase signals using the orthogonal demodulation method [23–30], which is totally the same as in the conventional coherent φ-OTDR systems.

The experimental setup of our φ-OTDR system is shown in Fig. 3. A narrow line-width laser (NLL) is used as the light source. The laser light is divided into two parts by a 10:90 optical coupler (OC1). Then 10% of the light is used as the local light to perform a coherent detection, and 90% of the light is modulated into optical pulses with a 200 MHz frequency shift by an AOM. After being amplified by an erbium-doped fiber amplifier (EDFA), the probe pulses are launched into an optical circulator (Cir). The Rayleigh backscattering light returned from the sensing fiber then interferes with the local light at a 50:50 optical coupler (OC2) and results in a beat light. The beat light is then detected by a BPD through a differential way, which could improve the SNR by 3 dB [34]. The output electric signal from the BPD is then filtered by a bandpass filter whose central frequency, bandwidth (FWHM), and stop-band rejection is 200 MHz, 15 MHz, and 40 dB, respectively. The bandpass signal is finally sampled by an 8-bit DAQ whose analog input bandwidth is 240 MHz. The pulse repeat frequency and pulse width used in our system is 3 kHz and 100 ns, respectively, which means that the FWHM of the beat signal spectrum is around 9 MHz. Two piezoelectric ceramic transducers (PZTs) with a 2 m fiber wound are separately put at approximately 4.86 km and 5 km over a 5.1 km sensing fiber as vibration sources, which are driven by an electrical signal generator (ESG).

To evaluate the impact of undersampling on the DAS signal demodulation, we conducted two experiments using different sampling frequencies. In one experiment, we sampled the beat signal with a sampling frequency of 91 MSa/s, which indicates a normal placement ($n = 5$) of the beat signal spectrum. We applied a 5–300 Hz chirp signal on the PZT2 as a vibration source. The locating result based on amplitude signals by using the moving average and differential method [34] is shown in Fig. 4(a). The moving average time used here is 10. After locating the vibration source, its phase signal can be demodulated. Both

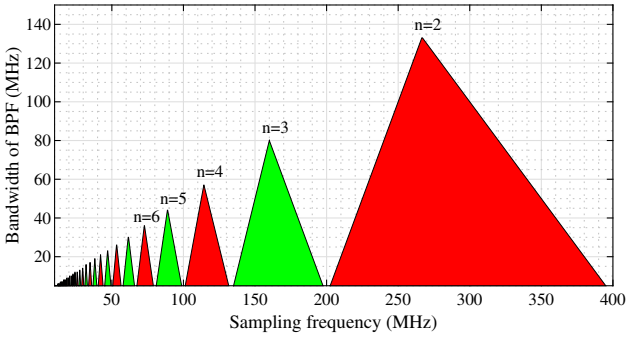

Fig. 2. Allowed areas of sampling frequency together with BPF bandwidth when the frequency shift induced by AOM is 200 MHz. Red area, normal spectrum placement after sampling; green area, inverse spectrum placement after sampling.

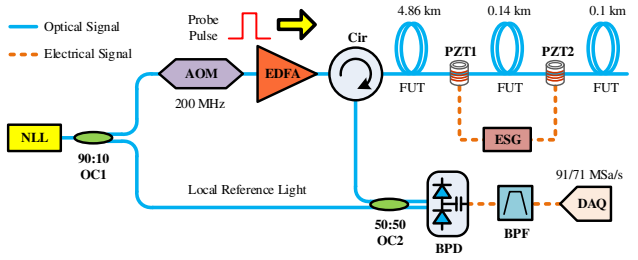

Fig. 3. Experimental setup. NLL, narrow line-width laser; OC, optical coupler; AOM, acousto-optic modulator; EDFA, erbium-doped fiber amplifier; Cir, circulator; FUT, fiber under test; PZT, piezoelectric ceramic transducer; ESG, electrical signal generator; BPD, balanced photodetector; BPF, bandpass filter; DAQ, data acquisition card.

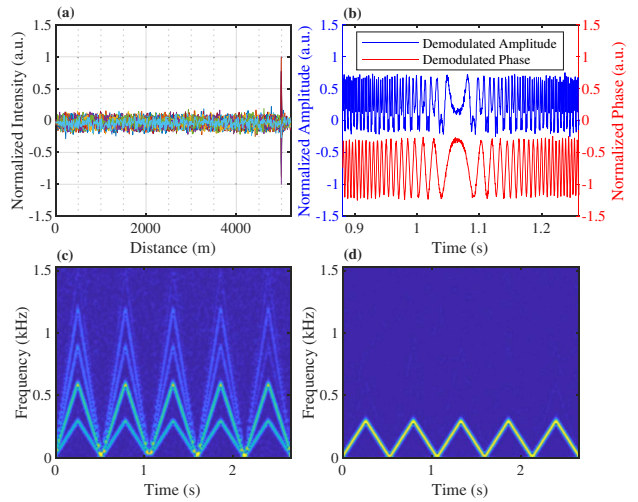

Fig. 4. Results of sampling the 200 MHz beat signal with a sampling rate of 90 MSa/s. (a) Vibration locating result based on amplitude signals. (b) Demodulated amplitude (blue line) and phase (red line) of the 5–300 Hz chirp vibration signal. Spectrograms of the demodulated (c) amplitude and (d) phase signals.

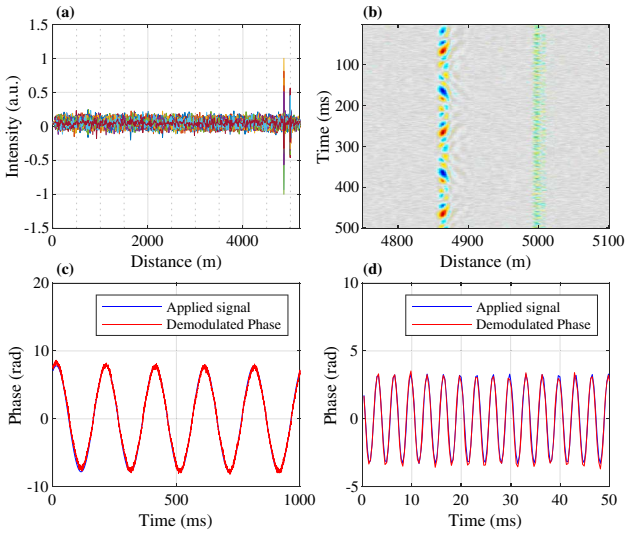

Fig. 5. Results of sampling the 200 MHz beat signal with a sampling rate of 71 MSa/s. Locating results based on amplitude signals visualized in (a) 1D and (b) 2D. Applied vibration signal (blue line) and demodulated phase signal (red line) of (a) PZT1 and (d) PZT2.

of the demodulated amplitude and phase signals that are induced by the PZT vibration are shown in Fig. 4(b). Figures 4(c) and 4(d) show the spectrograms of the amplitude and phase signal, respectively. We can see that the amplitude signal has a severe nonlinear effect, whereas the phase signal almost does not.

It the other experiment, we sampled the beat signal with a sampling frequency of 71 MSa/s, which indicates an inverse placement ($n = 6$) of the beat signal spectrum. This time we applied a 5 Hz single frequency signal and a 300 Hz single frequency signal, respectively, on the PZT1 and PZT2. The locating results based on the amplitude signals are shown in Figs. 5(a) and 5(b). The applied vibration signals on the PZTs and the demodulated phase signals are shown in Figs. 5(c) and 5(d). We can see that both the vibration sources are simultaneously located and well recovered, indicating that this method can be extended to detect multiple vibration events along the sensing fiber as well as capture its accurate phase change. In addition, the results prove that inverse spectrum placement of the beat signal is also acceptable for DAS signal demodulation.

In conclusion, we introduce an undersampling method for DAS systems based on a coherent φ-OTDR. Compared to the conventional phase-measuring coherent φ-OTDR, undersampling can reduce the amount of raw data by tens of times due to the low sampling frequency, meaning that the data processing burden can be sharply reduced. We also give the principle of selecting the correct sampling frequency and bandpass filter. The out-of-band noise may degrade the SNR due to aliasing; thus, the stop-band rejection of the BPF should be as high as possible. Experimental results show that the acoustic signals can be well recovered using this method. Owing to the low sampling frequency requirement, this method is expected to facilitate the practical application of DAS systems based on the coherent φ-OTDR.

Funding. National Natural Science Foundation of China (NSFC) (61627816, 61773059).

REFERENCES

1. J. C. Juarez and H. F. Taylor, J. Lightwave Technol. **23**, 2081 (2005).
2. J. C. Juarez and H. F. Taylor, Appl. Opt. **46**, 1968 (2007).
3. H. F. Martins, S. Martin-Lopez, P. Corredera, M. L. Filograno, O. Frazao, and M. Gonzalez-Herraez, J. Lightwave Technol. **31**, 3631 (2013).
4. F. Peng, H. Wu, X. H. Jia, Y. J. Rao, Z. N. Wang, and Z. P. Peng, Opt. Express **22**, 13804 (2014).
5. Y. Koyamada, M. Imahama, K. Kubota, and K. Hogari, J. Lightwave Technol. **27**, 1142 (2009).
6. L. Zhou, F. Wang, X. Wang, Y. Pan, Z. Sun, J. Hua, and X. Zhang, IEEE Photon. Technol. Lett. **27**, 1884 (2015).
7. J. Pastor-Graells, H. F. Martins, A. Garcia-Ruiz, S. Martin-Lopez, and M. Gonzalez-Herraez, Opt. Express **24**, 13121 (2016).
8. A. Garcia-Ruiz, J. Pastor-Graells, H. F. Martins, K. H. Tow, L. Thévenaz, S. Martin-Lopez, and M. Gonzalez-Herraez, Opt. Express **25**, 1789 (2017).
9. R. Posey, G. A. Johnson, and S. T. Vohra, Electron. Lett. **36**, 1688 (2000).
10. A. Masoudi, M. Belal, and T. P. Newson, Meas. Sci. Technol. **24**, 085204 (2013).
11. C. Wang, C. Wang, Y. Shang, X. Liu, and G. Peng, Opt. Commun. **346**, 172 (2015).
12. A. Masoudi and T. P. Newson, Opt. Lett. **42**, 290 (2017).
13. G. Fang, T. Xu, S. Feng, and F. Li, J. Lightwave Technol. **33**, 2811 (2015).
14. Y. Shang, Y. Yang, C. Wang, X. Liu, C. Wang, and G. Peng, Measurement **79**, 222 (2016).
15. S. Ying, Y. Yuan-Hong, W. Chen, L. Xiao-Hui, W. Chang, and P. Gang-Ding, Meas. Sci. Technol. **27**, 065201 (2016).
16. A. E. Alekseev, V. S. Vdovenko, B. G. Gorshkov, V. T. Potapov, and D. E. Simikin, Laser Phys. **24**, 115106 (2014).
17. A. E. Alekseev, V. S. Vdovenko, B. G. Gorshkov, V. T. Potapov, and D. E. Simikin, Laser Phys. **25**, 065101 (2015).
18. X. He, S. Xie, F. Liu, S. Cao, L. Gu, X. Zheng, and M. Zhang, Opt. Lett. **42**, 442 (2017).
19. S. Liehr, Y. S. Muanenda, S. Münzenberger, and K. Krebber, Opt. Express **25**, 720 (2017).
20. Y. Muanenda, S. Faralli, C. J. Oton, and F. Di Pasquale, Opt. Express **26**, 687 (2018).
21. Z. Wang, L. Zhang, S. Wang, N. Xue, F. Peng, M. Fan, W. Sun, X. Qian, J. Rao, and Y. Rao, Opt. Express **24**, 853 (2016).
22. Z. Sha, H. Feng, and Z. Zeng, Opt. Express **25**, 4831 (2017).
23. Z. Pan, K. Liang, Q. Ye, H. Cai, R. Qu, and Z. Fang, Proc. SPIE **8311**, 8311 (2011).
24. G. Tu, X. Zhang, Y. Zhang, F. Zhu, L. Xia, and B. Nakarmi, IEEE Photon. Technol. Lett. **27**, 1349 (2015).
25. G. Yang, X. Fan, S. Wang, B. Wang, Q. Liu, and Z. He, IEEE Photon. J. **8**, 1 (2016).
26. Y. Dong, X. Chen, E. Liu, C. Fu, H. Zhang, and Z. Lu, Appl. Opt. **55**, 7810 (2016).
27. F. Pang, M. He, H. Liu, X. Mei, J. Tao, T. Zhang, X. Zhang, N. Chen, and T. Wang, IEEE Photon. Technol. Lett. **28**, 2752 (2016).
28. G. Tu, B. Yu, S. Zhen, K. Qian, and X. Zhang, IEEE Photon. J. **9**, 1 (2017).
29. H. Liu, F. Pang, L. Lv, X. Mei, Y. Song, J. Chen, and T. Wang, IEEE Photon. J. **10**, 1 (2018).
30. Z. Zhong, F. Wang, and X. Zhang, IEEE Photon. J. **10**, 1 (2018).
31. P. Healey, Electron. Lett. **20**, 30 (1984).
32. J. D. Gaskill, *Linear Systems, Fourier Transforms, and Optics* (Wiley, 1978).
33. J. Liu, X. Zhou, and Y. Peng, IEEE Trans. Signal Process. **49**, 1260 (2001).
34. Y. Lu, T. Zhu, L. Chen, and X. Bao, J. Lightwave Technol. **28**, 3243 (2010).